PLOS One

RESEARCH ARTICLE

Computational insights into flavonoids inhibition of dengue virus envelope protein: ADMET profiling, molecular docking, dynamics, PCA, and end-state free energy calculations

Amar Waiba[1☯], **Anuraj Phunyal**[1☯], **Tika Ram Lamichhane**[2☯], **Madhav Prasad Ghimire**[2], **Hari Nyaupane**[1], **Ashish Phuyal**[1], **Achyut Adhikari**[1☯*]

1 Central Department of Chemistry, Tribhuvan University, Kirtipur, Kathmandu, Nepal, **2** Central Department of Physics, Tribhuvan University, Kirtipur, Kathmandu, Nepal

☯ These authors contributed equally to the work.
* achyutraj05@gmail.com

OPEN ACCESS

Citation: Waiba A, Phunyal A, Lamichhane TR, Ghimire MP, Nyaupane H, Phuyal A, et al. (2025) Computational insights into flavonoids inhibition of dengue virus envelope protein: ADMET profiling, molecular docking, dynamics, PCA, and end-state free energy calculations. PLoS One 20(7): e0327862. https://doi.org/10.1371/journal.pone.0327862

Editor: Yusuf Oloruntoyin Ayipo, Kwara State University, NIGERIA

Received: March 24, 2025

Accepted: June 20, 2025

Published: July 9, 2025

Peer Review History: PLOS recognizes the benefits of transparency in the peer review process; therefore, we enable the publication of all of the content of peer review and author responses alongside final, published articles. The editorial history of this article is available here: https://doi.org/10.1371/journal.pone.0327862

Abstract

Dengue virus is a critical worldwide health concern, and efforts to identify useful antiviral drugs remain imperative. This study utilized computational techniques to investigate the flavonoids as a potential inhibitor of the dengue virus envelope protein (PDB ID: 1OKE). 33 flavonoids were docked among them, 5-hydroxy-3-(4-hydroxyphenyl)-7-[(2S, 3R, 4S, 5S, 6R)-3,4,5-trihydroxy-6-(hydroxymethyl)oxan-2-yl]oxychromen-4-one (FLA1) showed the best binding affinity of -9.1 kcal/mol towards the E protein. Molecular dynamics simulations (100 ns) were carried out to analyze the stability and interaction of protein-ligand complexes, including parameters such as RMSD (FLA1 of 2.36 ± 0.43 Å), RMSF, Rg, SASA, hydrogen bonding, and RDF. In addition, PCA and DCCM analysis exposed considerable conformational differences and residue correlations favoring FLA1 stability. The binding free energy calculations using the MM/PBSA methodology confirmed the strong binding (-29.1 ± 5.83 kcal/mol) of FLA1 to the target protein. ADMET profiling also revealed good pharmacokinetic properties. These findings suggest FLA1 is a possible inhibitor of the dengue virus and a promising drug candidate for the development of antiviral drugs in the future.

1. Introduction

An infected mosquito transmits Dengue virus (DENV) (pathogen of the *Flaviviridae* family) and is responsible for widespread infection globally each year, particularly in tropical and subtropical areas [1–3]. The estimated global economic burden of dengue is around USD 8.9 billion annually [4]. Thus, it is crucial to prevent and treat these arboviral infectious diseases [5]. The range of health effects of DENV infection includes dengue fever (DF), which progresses into dengue hemorrhagic fever (DHF) in some patients, and in severe cases, dengue shock syndrome (DSS) [6].

Data availability statement: All relevant data underlying the finding of this study are now publicly available via Figshare repository https://doi.org/10.6084/m9.figshare.29205689.v1; https://doi.org/10.6084/m9.figshare.29206427.v1 for the replicate the results reported in this article.

Funding: The author(s) received no specific funding for this work.

Competing interests: No authors have competing interests.

At present, no specific antiviral treatment is available for dengue. Under medical supervision, people with dengue fever should get enough sleep, drink lots of fluids to stay hydrated, and take paracetamol to treat their illness. Though there are abundant possible antiviral candidates, only a few, such as celgosivir, lovastatin, prednisolone, balapiravir, and chloroquine, have undergone clinical trials [7,8]. There is currently only one approved dengue vaccine (CYD-TDV, Dengvaxia), developed by Sanofi Pasteur and comprising four shorts in total (CYD-1–4), which is used in some countries [9,10]. However, concerns about its general effectiveness among people [11]. Therefore, a pressing need remains to explore new therapeutic candidates that target the dengue virus.

The genome of DENV comprises a single positive-sense strand of whole Ribonucleic Acid (RNA), measuring 11 kb in size. The RNA genome consists of an individual open reading frame (ORF) bordered by untranslated places (UTRs) [12]. This ORF encodes a polyprotein, which is later cleaved into proteins that are structural and nonstructural; the structural proteins include pre-membrane (prM), envelope (E), and Core or capsid (C), while the nonstructural proteins consist of NS1, NS2A, NS2B, NS3, NS4A, NS4B, and NS5. Nonstructural proteins are crucial for processes such as viral RNA replication and evading the host immune system. In contrast, structural proteins are responsible for functions such as receptor binding, fusion, maturation, and assembly of DENV [13,14]. E protein consists of 394 amino acid residues made from the three structural parts, Domain I, II, and III [15]. Domain II (DII) contains the fusion peptide loop, which facilitates E to insertion into the host cell membrane, but when pH alters, its structural integrity where Domain III (DIII) plays a role in receptor binding (Fig 1) [16].

The dengue virus E protein's complicating structural changes stimulate the joining of the viral envelope and cell membranes. Initially, the acidic environment of the endosome and a specific histidine residue in E undergo protonation, prompting the reversible separation of protein dimers of the virion surface [17,18]. This procedure, made possible by DII's flexible movement around a hing domain at Domains I and II intersections, exposes the fusion peptide loop at the end of Domain II (DII) and permits entry into the host cell membrane [19–21]. During this transformation, the E protein acts as a bridge that connects the viral envelope with the cellular membrane, and the homotrimers of E proteins are formed permanently [22,23]. Thus, the E protein in the design of DENV entry inhibitors is one of the more promising methods for

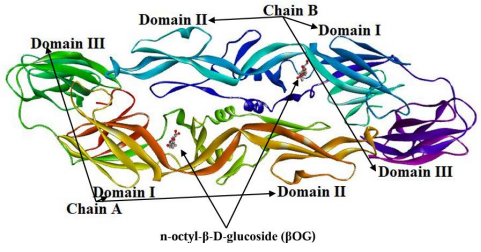

Fig 1. Cartoon representation of envelope protein showing chain A, chain B, Domains, and βOG.

https://doi.org/10.1371/journal.pone.0327862.g001

inhibiting the virus. In recent *in silico* screenings, most inhibitors target the n-octyl-β-glucoside (βOG; native ligand) pocket as a binding site [20].

Flavonoids are polyphenolic compounds found in several plant species with various properties, such as antiviral, antioxidant, antibacterial, and antimutagenic [24–27]. Previous studies have reported several flavonoids as inhibitors of dengue through various mechanisms. However, a systematic evaluation of flavonoids targeting the DENV E protein remains limited.

In this study, we made a database of flavonoids (*ca.* 3000 compounds) based on literature reports on their antiviral activity, structural diversity, and drug-likeness profiles [28–30]. The main goal was to explore the inhibitory effects of flavonoids against an envelope inhibitor among the tested molecules. By utilizing molecular docking, molecular dynamics simulations, and free energy calculations, we predict where the flavonoids bind to the E protein structure, assess their interaction and stability in the orthosteric site, and determine the drug-likeness properties of flavonoids. The compound FLA1 emerged as a promising hit for further investigation. This work provides preliminary computational insights into flavonoid-based E protein inhibition and lays the groundwork for future *in vitro* and *in vivo* validation.

2. Material and methods

2.1. Selection and preparation of ligand database

A curated database of compounds (*ca.* 3000 flavonoids) was obtained from different literature sources. The 3D structures of these compounds retrieved from the PubChem website (https://pubchem.ncbi.nlm.nih.gov/) in SDF format. The ligands preparation involved adding polar hydrogens, energy minimization, and verification of molecular formulas using the Avogadro software v1.1 [31]. The resulting structures were then converted from SDF to PDB fotmat using PyMOL v2.5.4 for molecular docking studies [32].

2.2. Protein preparation and validation

The DENV E protein was selected as a target, corresponding to PDB ID 1OKE (Expression organism: *Drosophila melanogaster*) (https://doi.org/10.2210/pdb1OKE/pdb) [20]. Its crystal structure, which has 394 amino acid residues and a resolution of 2.40 Å, was obtained from the Protein Data Bank web server (https://www.rcsb.org/). The structure includes two chains (A and B), with chain A selected for further studies. PyMOL v2.5.4 was employed to remove chain B, water molecules, and co-crystallized ligands, and adding hydrogen atoms to prepare the protein structure for analysis. Subsequently, AutoDockTools v1.5.7 introduces a Kollman charge of -84.799, ensuring system neutrality and converting the PDB to PDBQT format [33]. The structure analysis and validation of the protein using the SAVES v6.0 web server (http://saves.mbi.ucla.edu/) provides three different applications: ERRAT, VERIFY 3D, and PROCHECK [34].

2.3. ADMET prediction

The multiple web servers (ADMETlab2.0, ProTox-II, pkCSM, and swissADME) were used to evaluate the pharmacokinetic and pharmacodynamic properties of compounds [35–38].

2.4. Molecular docking

The Autodock Vina software v1.2 was used for molecular docking, which is based on the Lamarckian Genetic Algorithm (LGA) and used to generate AutoGrid and grid maps with X = 40 Å, Y = 40 Å, and Z = 40 Å as typical grid box sizes, the energy range of 3, spacing of 0.375, and 20 modes with exhaustiveness of 32, the grid center dimensions set at X = -12.964, Y = 80.186, and Z = 45.884, after that, perform docking on the βOG pocket (orthosteric site) and confirmed active sites of proteins using CASTp server [39,40]. The top three protein-ligand complexes (according to their binding affinity) were saved in PDB format and then converted into PDBQT for molecular dynamics simulations. Visualizing the binding interaction between protein and ligand using the Discovery Studio 2021 program [41].

2.5. Molecular dynamics simulation

The GROMACS program simulated the best binding affinity complexes obtained after molecular docking [42]. The Charmm27 force field was used for receptor topology due to its compatibility with ligand topology files [43]. The SwissParam web server (http://swissparam.ch/) was used for ligand force field in the.zip format [44]. For solvation of the system, the TIP3P water model within a triclinic box (a = 5.86 nm,b = 7.34 nm, c = 14.39 nm) with a spacing of 10 Å at the sides was chosen to prevent interactions between the periodic images. The system was neutralized by adding a 0.15 M NaCl solution. Equilibration was executed in four phases, each lasting 200 ps, which were used in the equilibration procedure, which was carried out at 310 K, the physiological temperature. In the first two stages, the equilibrium was reached at constant temperature and volume (NVT), while the subsequent two steps attained equilibrium under constant pressure and temperature (NPT). During equilibration, temperature coupling was utilized for the modified Berendsen thermostat, and pressure coupling was performed using the Berendsen method. Particle Mesh Ewald (PME) was utilized to manage distant coulomb interactions [45]. After equilibration, a 100 ns production run was carried out without restraints with a step size of 2 fs. Using inbuilt modules, several geometrical parameters were tracked during these simulations, including Root Mean Square Deviation (RMSD), Root Mean Square Fluctuation (RMSF), Radius of Gyration (Rg), Solvent Accessible Surface Area (SASA), Hydrogen bond count, Radial Distribution Function (RDF), Principle Component Analysis (PCA), and Dynamic Cross-Correlation Matrix (DCCM).

2.6. Binding free energy calculation

The gmx_MMPBSA module of GROMACS computes the binding free energy of the complexes over the final 10 ns equilibrated trajectories and was thoroughly described in Phunyal et al. [46].

2.7. DCCM and PCA calculations

The R programming package Bio3D was used to perform DCCM and PCA analysis from MD trajectories. A detailed protocol was outlined at Gyawali et al. [47].

3. Results

3.1 Validation of protein structure and analysis

Before conducting molecular docking, the E protein underwent preparation and validation through server analysis. The protein's ERRAT score was determined to be 84.6154, showing favorable quality, while from the VERIFY module, its structural integrity was 82.23%. Based on a complex deposited in a protein data bank, analysis of the active site identified **GLN271, GLU49, THR48, ALA50, LEU198, ILE270, PHE193, LEU207, PHE297, THR280, VAL130, LEU135, GLN200, SER274, ALA205, and LEU277** amino acid residues interacting via hydrogen bonding, Van der Waals', Carbon hydrogen bond, Alkyl, pi-Alkyl. The Ramachandran plot from the PROCHECK module of the SAVES server illustrates the configurations of phi (ϕ) and psi (ψ) angles within a polypeptide. Approximately 81.8% of residues occupy the most favored regions on this plot (S1 Fig). Another 17.6% fall within the additional allowed region, leaving only 0.6% in the disallowed regions. This distribution suggests a well-constructed protein model with high-performance expectations.

3.2 Validation of molecular docking

The native ligand was re-docked to the protein, and less than 1.912 Å of RMSD relative to the co-crystal pose in the crystal structure showed molecular docking was valid [48]. The parameters were chosen to validate docking for other ligands (Fig 2).

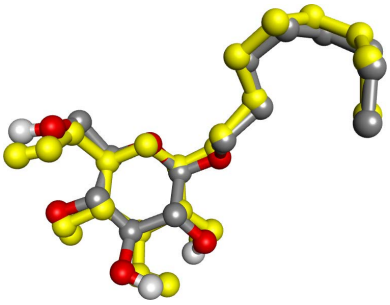

Fig 2. Docking validation. Binding interactions between the first docked βOG (grey), sourced from PDB, and the re-docked βOG (yellow) ensure an RMSD of less than 2 Å.

https://doi.org/10.1371/journal.pone.0327862.g002

3.3 Drug-likeness and ADMET profiling

Out of *ca.* 3000 flavonoids screened, only 33 passed toxicity criteria (hepatotoxicity, carcinogenicity, mutagenicity, immunotoxicity, and cytotoxicity). The hit candidates are classified as class 4–6 and have LD_{50} values over 2000 mg/kg, indicating they have low acute toxicity (S1 Table). Regarding drug-likeness, the physicochemical properties of hit candidates are in an acceptable range and adhere to Lipinski's rule of five (1 violation; FLA1) and Veerber's criteria (S2 Table). Pharmacokinetically, the compounds had a good plasma protein binding (PPB) range between 71% and 98%, suggesting a favorable therapeutic index and prolonged systemic circulation (S3 Table).

Regarding safety, the hit candidates demonstrated acceptable results for skin sensitization (0 to 0.8) and low eye corrosion or irritation, which indicated a low risk of dermal and ocular toxicity (S4 Table). Similarly, blood bank barrier (BBB) permeability value of <-3 logPS < -3 categorizes them as CNS-impermeable. While such CNS non-penetrance could also be a limitation in other applications, if targeting the nervous system is not desired in the treatment of dengue (where CNS effects are undesirable), a limited BBB permeability may be an advantage for reducing off-target neurotoxicity.

Furthermore, the candidates were found to possess a low gastrointestinal (GI) toxicity and were unable to inhibit major cytochrome P450 enzymes (CYP2D6, CYP1A2, CYP1A2, CYP2C19, CYP2C9, and CYP3A4), which suggests low metabolic interaction risk [49]. The flavonoids were also not identified as substrates for renal Organic Cation Transporter 2 (OCT2), suggesting minimal interference in renal clearance mechanisms (S5 Table). Compared to a reference ligand (NITD448) (class 5, LD_{50} = 2150 mg/kg), it showed immunotoxicity, did not follow Lipinski's rule of five, and did not follow Verber's rule. Similarly, it showed greater PPB (99.18%). Therefore, the chosen hit candidates possess an acceptable ADMET profile.

3.4 Molecular docking analysis

Molecular docking was used for molecular interactions of different protein-ligand complexes at a molecular level. Using AutoDock Vina, molecular docking was carried out on the βOG pocket of the dengue virus's E protein. This investigation contains 33 flavonoids, native ligands, and NITD448 (reference ligand). We examined these chemical binding affinities with E protein and studied how they interact with hydrophobic areas. When compared to the native ligand (-5.7 kcal/mol) and reference ligand (-8.1 kcal/mol), all 33 flavonoids showed lower binding affinities (ranging from -9.1 to -6.8 kcal/mol) (Table 1).

Among 33 flavonoids, the top three compounds with the highest binding affinities were studied for further calculations (S2 Fig). The molecular details of different flavonoids bonding interactions with key amino acid residues and their distance have been obtained (Table 2). FLA1 exhibits the best binding affinity among the compounds, which have a binding energy of -9.1 kcal/mol. Key amino acid residues including **THR48** (4.21 Å), **ALA50** (3.64 Å), and **THR280** (**3.04 Å**) interact with

Table 1. Ligands with its binding affinity.

S.N	Flavonoids (PubChem CID)	Representative name	Binding affinity (Kcal/mol)
1	5281377	FLA1	-9.1
2	5281607	FLA2	-8.6
3	442520	FLA3	-8.6
4	5322064	FLA4	-8.6
5	5281616	FLA5	-8.5
6	5320315	FLA6	-8.4
7	5281611	FLA7	-8.4
8	5280443	FLA8	-8.3
9	5280863	FLA9	-8.3
10	5280666	FLA10	-8.2
11	5281612	FLA11	-8.2
12	5281628	FLA12	-8.1
13	1203	FLA13	-8.1
14	12912214	FLA14	-8.0
15	5319484	FLA15	-8.0
16	5280637	FLA16	-7.8
17	5280373	FLA17	-7.7
18	11449086	FLA18	-7.6
19	5280457	FLA19	-7.6
20	5281708	FLA20	-7.6
21	182232	FLA21	-7.5
22	6453244	FLA22	-7.5
23	5280961	FLA23	-7.5
24	5320946	FLA24	-7.5
25	5281804	FLA25	-7.5
26	1226045	FLA26	-7.4
27	5282102	FLA27	-7.3
28	5281702	FLA28	-7.3
29	5272653	FLA29	-7.2
30	5322078	FLA30	-6.8
31	5468749	FLA31	-6.8
32	5281703	FLA32	-6.8
33	631095	FLA33	-6.8
34	62852	Native ligand (βOG)	-5.7
35	139031065	NITD448 (Reference drug)	-8.1

https://doi.org/10.1371/journal.pone.0327862.t001

FLA1 through hydrogen bonding, while additional interactions like Van der Waals' force of attraction (**ALA205**, **GLN200**, **SER274**, LYS47, **GLU49**, **LEU277**, **PHE193**, LEU191, GLY281, GLY190, **PHE279**, THR268), Pi-Sigma (**LEU 207**) (Fig 3a). FLA2 exhibits a slightly higher binding affinity of -8.6 kcal/mol. Like, FLA2 interacts with hydrogen bonding through **ALA50** (**3.39** Å), **GLN200** (4.49 Å), and **GLN271** (3.84 Å), amino acid residues. In addition, other interactions such as Pi-Alkyl (**LEU198**, **ILE270**), and Van der Waals' (**PHE193**, **THR280**, **THR48**, **GLU 49**, **LEU277**, ASP203) (Fig 3b). Similarly, FLA3 demonstrates binding affinities similar to FLA2, which is -8.6 kcal/mol. In the case of FLA3, displayed interactions by hydrogen bonding by **ALA50** (**3.34** Å) amino acid residue. Additional bonds like Pi-Alkyl (**ILE270**, **LEU198**), and Van der Waals' (**PHE193**, **THR280**, **THR48**, **GLU49**, **LEU277**, **GLN271**, **GLN200**) (Fig 3c). Interaction of native ligand

Table 2. Key amino acids and various interaction types among the top 3 candidates.

Compounds PubChem CID (Representative Name)	Interactions	Key amino acid residues with distance (Å)
	H-bonding	**THR280** (**3.04**), **THR48** (4.21), **ALA50** (3.64)
5281377 (FLA1)	pi-sigma	**LEU207** (4.82)
	Van der Waals'	**ALA205**, **GLN200**, **SER274**, LYS47, **GLU49**, **LEU277**, **PHE193**, LEU191, GLY281, GLY190, **PHE279**, THR268
	H-bonding	**GLN200** (4.49), **GLN271** (3.84),**ALA50 (3.39)**
5281607 (FLA2)	pi-alkyl	**ILE270** (4.90), **LEU198** (4.91)
	Van der Waals'	**THR48**, **GLU49**, **LEU277**, ASP203, **THR280**, **PHE193**
	H-bonding	**ALA50 (3.34)**
442520 (FLA3)	pi-alkyl	**LEU198** (4.95), **ILE270** (4.98)
	Van der Waals'	**GLU49**, **LEU277**, **GLN271**, **GLN200**, **PHE193**, **THR280**, **THR48**
62852 (Native ligand)	H-bonding	**ALA50 (3.50)**
	pi-alkyl	**LEU207 (4.62), VAL130 (4.92), ILE (4.31)**
	Van der Waals'	**ALA205, GLN200, GLU49, LEU277, PHE279**, LEU135, THR280, GLN271
139031065 (Reference ligand)	H-bonding	THR268 (4.71), GLU269 (3.77)
	pi-alkyl, pi-sigma, pi-pi stacked	**LEU207 (4.93), ALA50 (4.44), LEU198 (4.52)**, ILE270 (4.34), LEU191 (4.77), PHE279 (4.53)
	Van der Waals'	MET196, HIS282, GLY281, **THR48, THR280, PHE193**, GLY190

https://doi.org/10.1371/journal.pone.0327862.t002

with hydrogen bonding through **ALA50** (**3.50 Å**); meanwhile, extra interactions such as Van der Waals' force of attraction (**ALA205, GLN200, GLU49, LEU277, PHE279**, LEU135, THR280, GLN271) and pi-alkyl (**LEU207, VAL130, ILE270**) (Fig 3d). Likewise, reference ligand exhibits interactions with hydrogen bonding through THR268 (4.71 Å) and GLU269 (3.77 Å) and additional interactions, including Van der Waals' force of attraction (MET196, HIS282, GLY281, **THR48, THR280, PHE193**, GLY190), Pi-alkyl (**LEU207, ALA50, LEU198, ILE270**), Pi-sigma (LEU191) and Pi-Pi stacked (PHE279) (Fig 3e). Previous studies using the same receptor reported similar active site residues, indicating that the calculations were consistent [50,51]. Distinct hydrophobic (non-covalent) and hydrophilic regions were identified for each of the four adducts through 3D interaction analysis (S3 Fig). The different coloured regions signify hydrophilicity (blue, which indicates a higher number of electronegative atoms) and hydrophobicity (brown, which indicates a smaller number of electronegative atoms) parts in the protein structure.

3.5 Molecular dynamics simulation analysis

3.5.1 Root mean square deviation (RMSD). The protein-ligand complexes' dynamic stability and conformational behaviour were analyzed using the RMSD curve of the ligand and protein backbone (Fig 4a and 4b). Overall, the ligand RMSD values remained below 5 Å (except FLA3), indicating that the ligands bind strongly at the orthosteric site throughout the 100 ns MDS. Notably, FLA1 and native ligand exhibited the lowest average RMSD values of 2.57 ± 0.46 Å and 2.20 ± 0.41 Å, respectively, suggesting a more stable interaction compared to FLA2 of 2.28 ± 0.72 Å, FLA3 of 3.65 ± 0.94 Å, and reference ligand of 3.99 ± 0.76 Å (Fig 4a). The higher fluctuation in FLA3 during the initial 20 ns of MDS, and afterwards, maintains an RMSD of 3.65 ± 0.94 Å.

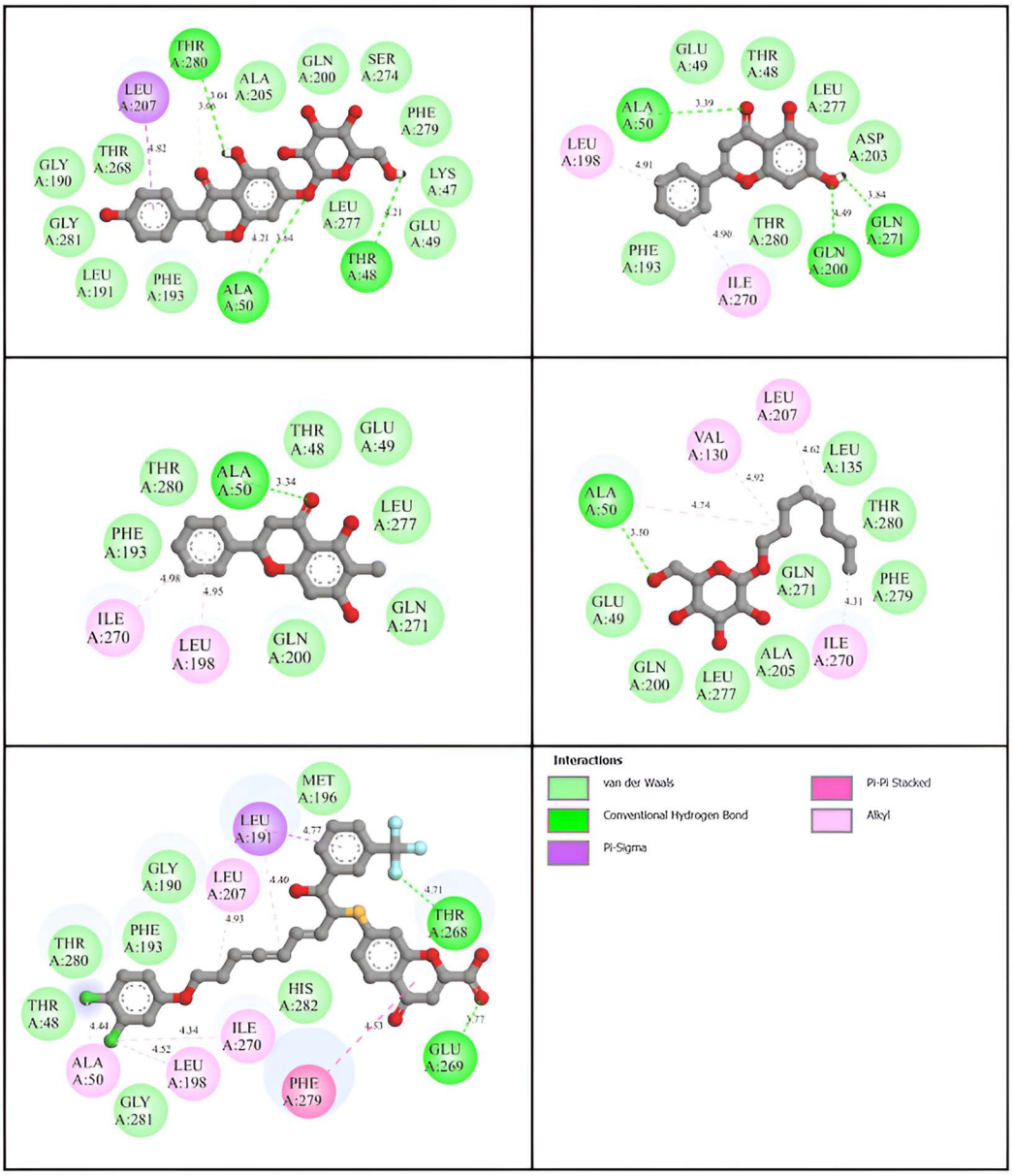

Fig 3. Two-dimensional projection of the protein-ligand interaction. (a) FLA1 (b) FLA2 (c) FLA3 (d) Native ligand (e) Reference ligand.

https://doi.org/10.1371/journal.pone.0327862.g003

The protein backbone RMSD profiles of protein-ligand complexes showed that protein-FLA1 complexes displayed smooth trajectories with RMSD of 2.36 ± 0.43 Å, Whereas FLA2, FLA3, and native ligand reveal the instability among which FLA3 expresses maximum shifts. Both of them attained stability after 25 ns, with a 3.83 ± 0.96 Å, 5.29 ± 1.74 Å, and 3.36 ± 0.79 Å, respectively. Likewise, the reference ligand shows fluctuation from 0 ns to 50 ns. That was due to the change in conformation of the ligand, and later on, it became smooth with 4.15 ± 0.76 Å (Fig 4b). Similar results were observed during the former work [50]. These differences in RMSD are functionally relevant, as ligand binding into the orthosteric pocket is intended to block the conformational transition of the DENV protein from dimer to trimer. Overall, the lowest RMSD value of ligand FLA1 suggests it can more effectively stabilize the conformation of the E protein.

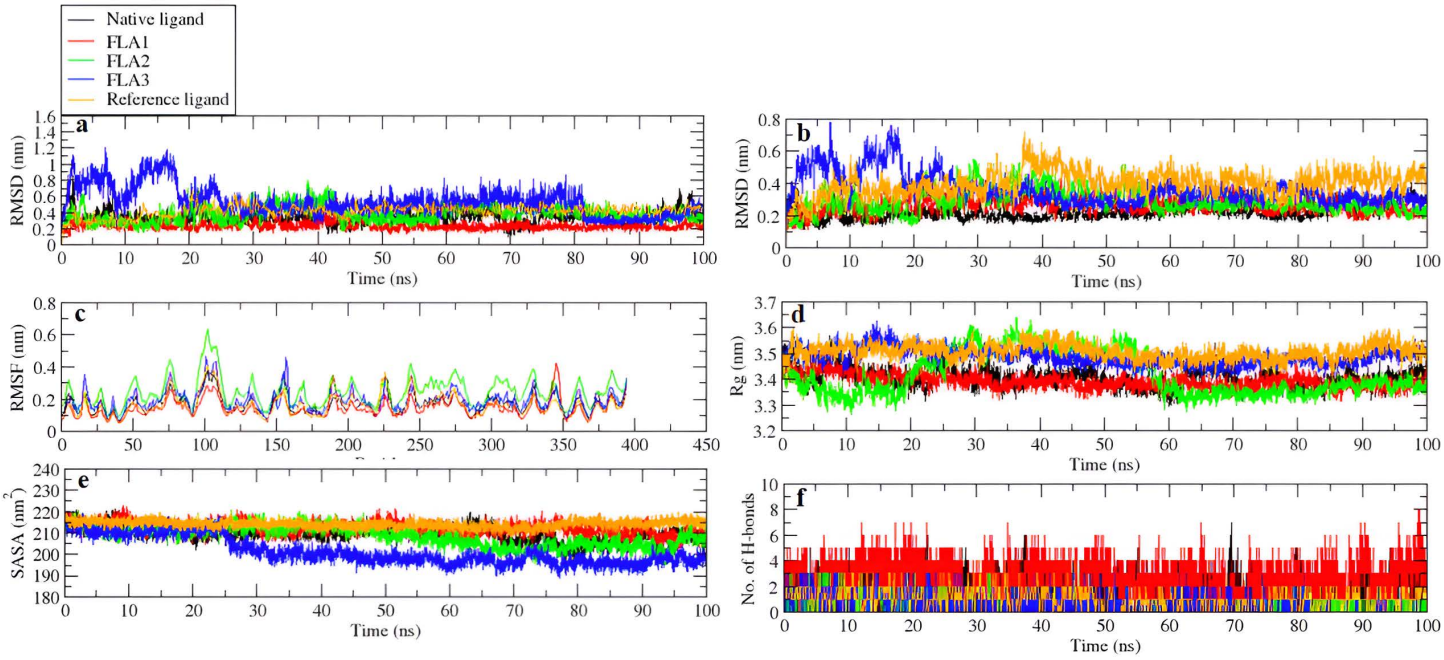

Fig 4. The RMSD of, (a) the protein backbone relative to the ligand (b) the protein backbone related to the protein backbone, c) The RMSF curves of the protein's α-carbon atoms, (d) The protein's Rg curves, (e) The SASA of the protein, and (f) The count of hydrogen bonds that bind ligands to proteins in various complexes derived from 100 ns MDS trajectories.

https://doi.org/10.1371/journal.pone.0327862.g004

3.5.2 Root mean square fluctuation (RMSF). The alpha carbon atoms RMSF of amino acid residues facilitates in evaluating how each amino acid's residues fluctuate when the ligand binds; the more stable the protein geometry, the lower the RMSF value (less than 5 Å) [52]. RMSF plots were generated from MDS for each complex, as shown (Fig 4c). The FLA2 and FLA3 complexes showed a greater fluctuation between 90–115 amino acid residues and a fluctuation of 2.44 ± 0.87 Å and 1.89 ± 0.66 Å, respectively. That is due to the region lacking beta sheet or alpha helix structures and having little to no interaction with the ligand; it seems that these variations have very small to no effect on the instability of the complex. Overall, FLA1, native ligand, and reference ligand show less fluctuation of 1.44 ± 0.55 Å, 1.69 ± 0.58 Å, and 1.63 ± 0.62 Å, respectively.

3.5.3 Radius of gyration (Rg). The Rg indicates the compactness of protein-ligand complexes; smaller Rg values indicate a more compact structure [53]. The FLA2 and FLA3 complexes displayed a significant expansion of the protein within an interval of 20 ns to 60 ns afterwards; they both exhibited smooth lines with a value of 34.17 ± 0.81 Å and 34.87 ± 0.30 Å, respectively. In comparison, the native ligand and reference ligand were found to be smooth curves with values of 34.05 ± 0.37 Å and 35 ± 0.29 Å, respectively. The FLA1 ligand complex showed a significant uniform trajectory of Rg of 33.92 ± 0.26 Å, indicating a slight rise of the protein upon ligand binding (Fig 4d).

3.5.4 Solvent accessible surface area (SASA). The protein's SASA facilitates identifying the total wettable area for protein throughout MDS. It was found to be 212.17 ± 2.7 nm^2, 208.52 ± 4.63 nm^2, 201.49 ± 6.45 nm^2, 209.87 ± 3.64 nm^2, and 214.20 ± 1.66 nm^2 in protein FLA1, FLA2, FLA3, native ligand, and reference ligand complexes, respectively (Fig 4e). The trajectory of the complex formation displayed reduced fluctuation for SASA, suggesting the complex's stability with a constant result in the surface area of the protein interacting with the solvent. The protein does not unfold or fold to indicate structural integrity, and its hydrophobic area is not exposed to the solvent molecules [54].

3.5.5 Hydrogen bond count. The total number of conventional hydrogen bonds in protein-ligand complexes affects the stability of the complex (Fig 4f). Stability increased through a rise in hydrogen bonds [55]. FLA1 displayed a maximum number

of eight hydrogen bonds, while the native ligand displays seven. In contrast, FLA2 and FLA3 exhibited three hydrogen bonds, while the reference ligand shows a minimum of two hydrogen bonds. The larger RMSD of FLA2 and FLA3, along with a smaller RMSD of FLA1 and the native ligand, was likely caused by the difference in hydrogen bond formation (Fig 4a).

3.5.6 Radial Distribution Function (RDF). Radial distribution functions (RDFs) of hydrogen bonding atom pairs between proteins and ligands observed during molecular dynamics (MD) simulations illustrate both sharp and broad peaks (Fig 5) [56]. Sharp RDF peaks indicated stronger hydrogen-bonding interactions, while broad RDF peaks showed weaker hydrogen bonding [57].

In FLA1, the atom pairs H1(FLA1)-O(THR48) and O2(FLA1)-HN(ALA50) displayed sharp peaks at 2.45 ± 0.56 Å and 2.5 ± 1.45 Å respectively, indicating strong hydrogen bonds. H(FLA1)-OG(THR280) showed a broader and lower peak at 6.85 ± 0.73 Å, suggesting a weaker interaction. For FLA2, the pairs of O1(FLA2)-HN(ALA50) and H1(FLA2)-OE1(GLN271) reveal distinct RDF peaks at 2.5 ± 0.53 Å and 1.95 ± 0.27 Å, respectively, indicating strong hydrogen bonding. Meanwhile,

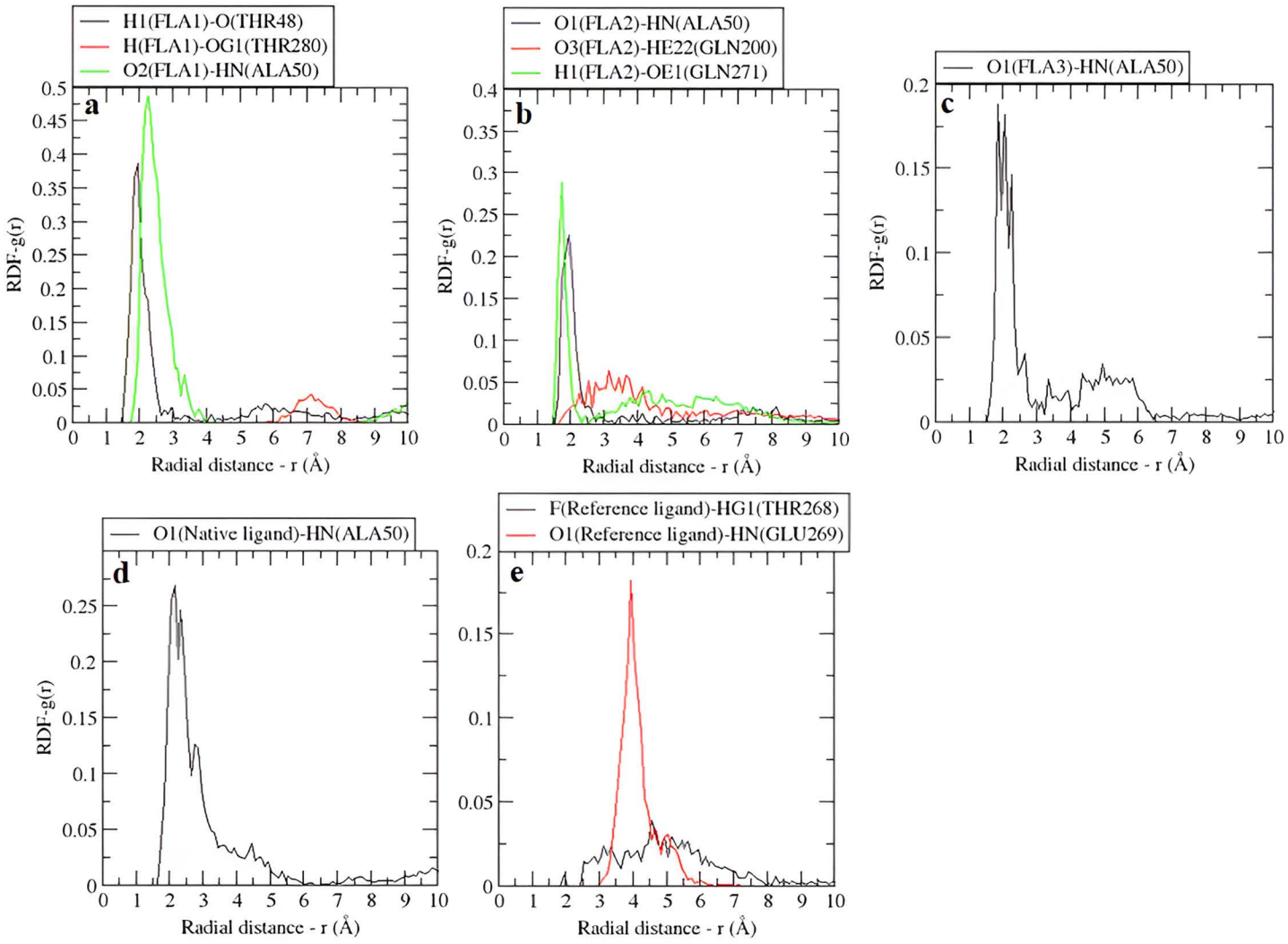

Fig 5. RDFs of highly interacting atom pairs among the ligand and protein residues that form H-bonds with each other in, (a) FLA1, (b) FLA2, (c) FLA3, (d) Native ligand, and (e) Reference ligand.

https://doi.org/10.1371/journal.pone.0327862.g005

the pair O3(FLA2)-HE22(GLN200) signified a wide and lower peak at 3.9 ± 1.28 Å, indicating weaker interaction. In FLA3, a single interaction between O1(FLA3)-HN(ALA50) produces a sharp yet slightly broad peak at 2.85 ± 0.73 Å, reflecting a moderate hydrogen bond. For the native ligand, the O1(Native ligand)-HN(ALA50) interaction produces a clear peak at 3.65 ± 1.14 Å, consistent with a stable hydrogen bond. Similarly, in the reference ligand, O1(Reference ligand)-HN(GLU269) generates a strong peak at 4.45 ± 0.85 Å, signifying a strong hydrogen bond, while F(Reference ligand)-HG1(THR268) showed a weaker, broader peak at 5.3 ± 1.63 Å, indicating a much weaker interaction. Overall, the FLA1 shows stronger hydrogen bonding with the E protein, to a greater extent, which can be verified from the hydrogen bond count, which has eight hydrogen bonds, which is the maximum among them.

3.5.7 Ligand snapshots at the protein's active site during simulations. To investigate the alignment (rotational motion) and location (translational motion) of these docked ligands, snapshots were taken at various instantaneous times of MDS (0, 25, 50, 75, and 100 ns) (Fig 6). With few exceptions, most ligands stayed in the same spot but had different orientations. In FLA1, the ligand exhibits exceptional data in which it remained in the same position as well as with the same orientation in the active site; also, in the case of the native ligand and reference ligand complexes, similar information was obtained but slightly changed in orientation; both of these details valid by smooth backbone protein-ligand RMSD. The ligand in the FLA2-protein complex stays in the same spot but has a different orientation. In the initial phase, the protein backbone in the FLA3-protein complex appears to undergo a substantial conformational shift, as evidenced

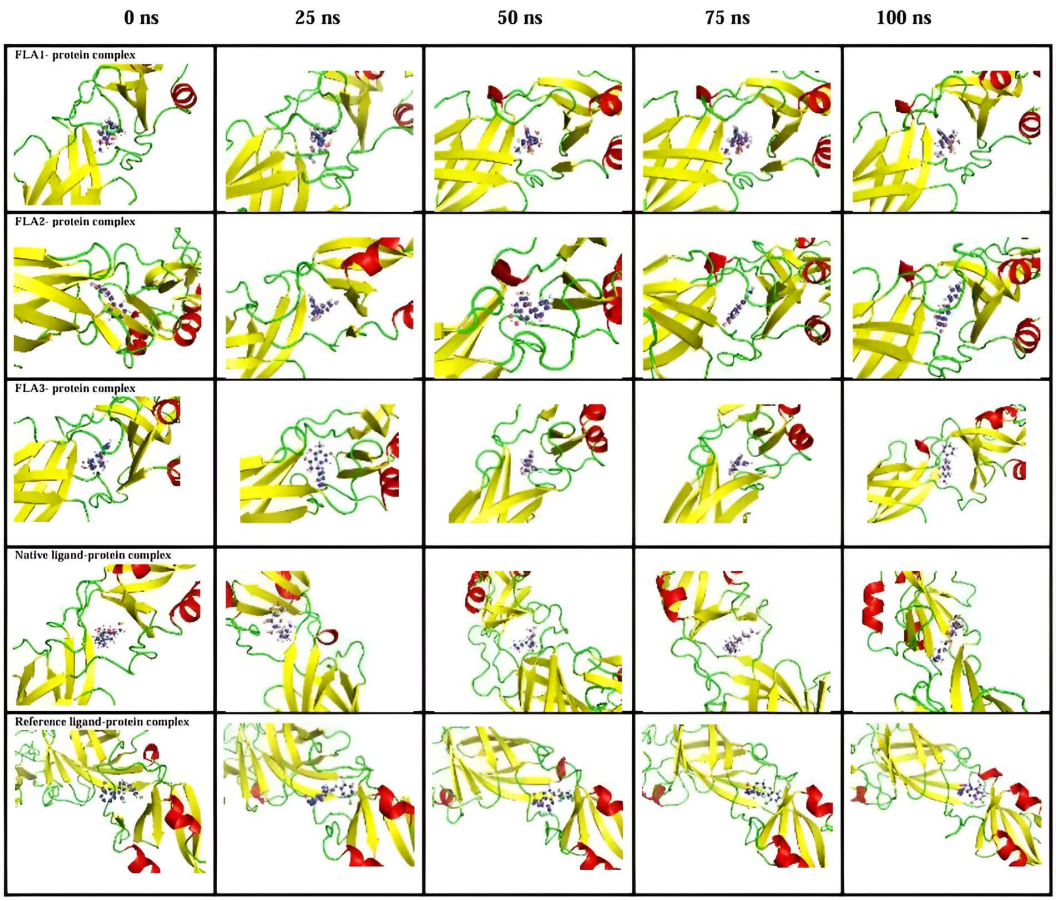

Fig 6. Images capturing the ligand's positioning at the orthosteric site during MDS. Orientation and location of ligands (shown in ball and stick model) to be monitored at various times.

https://doi.org/10.1371/journal.pone.0327862.g006

by the large spikes in the protein backbone RMSD curve. However, after 30 ns, the protein backbone stabilized. The evolution of different molecules linked to a structural description was clearly understood due to their dynamic behaviour being constantly observed.

3.5.8 PCA and DCCM analysis. PCA and DCCM of the different complexes were performed through 100 ns MDS trajectories (S4 and S5 Figs). In PCA analysis, different colours (blue, white, and red) indicated the different stages (initial, intermediate, and final time steps) of the ligand's conformation in the simulation period [58]. In protein-FLA2, PC1 clusters had the most significant level of variability (56.94%), followed by PC2 clusters (16.69%) and PC3 (9.78%) clusters (S4 Fig). The FLA1-protein and FLA2-protein complexes show greater shifts in PC1, PC2, and PC3 than native ligand-protein and reference ligand-protein complexes. In addition, eigenvalue distribution also confirmed these tendencies, observing the significance of PC1 in describing major structural dynamics.

The DCCM plots depict the correlation effects of amino acids in MDS trajectories (S5 Fig). The FLA1-protein exhibited maximum interaction with the best distribution of positive correlations (0–1) in major functional regions and stability with reduced negative correlations (−1–0). Similarly, the FLA2-protein complex also displayed positive correlations in the active site but with higher anti-correlations, indicating a loss of flexibility. In contrast, the FLA3-protein complex displayed a mix of strong positive and negative correlations, which showed allosteric effects but with some indication of structural instability. Similarly, the native ligand-protein and reference ligand-protein complex displayed weak correlations and scattered anti-correlations, which indicates destabilization.

3.6. Binding free energy analysis

The binding free energy (ΔG_{BFE}) and energy component analyses revealed protein-ligand interaction stability [59]. Among the ligands, FLA1-protein had the most favourable binding free energy (-29.1 ± 5.83 kcal/mol) (except reference ligand -40.21 ± 6.13 kcal/mol) than other protein-ligand complexes and protein-native complex (-18.94 ± 3.2 kcal/mol) (Table 3). In the energy vs. frames plot, FLA1-protein exhibited the most stable interaction throughout the simulation with minimal fluctuations (S6 Fig).

Van der Waals energy (VDWAALS), electrostatic energy (EEL), polar solvation energy (EPB), and nonpolar solvation energy (ENPOLAR) are the main contributors to the total binding free energy (S7 Fig). Decomposition of the energy terms revealed that reference ligand-protein complex had favourable van der Waals' (-53.32 ± 2.84 kcal/mol) and electrostatic (-24.49 ± 10.15 kcal/mol) interactions with some penalty for desolvation (ΔE_{PB} = 43.17 ± 5.57 kcal/mol) (S7 Fig). Residue decomposition analysis revealed that in the FLA1-protein complex, several active site residues namely THR48, GLU49, ALA50, LEU135, PHE193, LEU198, LEU207, GLN200, ILE270, GLN271, and LEU277, play a crucial role in the binding energy contributions. In contrast, for the reference ligand-protein complex, which exhibited a higher overall binding energy, the ligand interactions were primarily associated with VLA130, LEU198, ILE270, and LEU277 (S8 Fig). These findings were further supported by a heat map of complexes, where residue contributions are visually represented. In the heat map, darker blue colours correspond to residues with higher energy contributions. In contrast, lighter, faded colours indicated minimal involvement, confirming these residues' key roles in ligand binding (S9 Fig).

Table 3. The components of binding free energy change (ΔG_{BFE}: mean with standard deviation) for complexes.

Complexes	ΔE_{VDW}	ΔE_{EL}	ΔE_{PB}	ΔE_{NPOLAR}	ΔG_{GAS}	ΔG_{SOLV}	ΔG_{BFE}
FLA1-protein complex	−48.19 ± 3.07	−21.29 ± 8.89	44.96 ± 4.77	−4.59 ± 0.09	−69.47 ± 8.64	40.37 ± 4.77	−29.1 ± 5.83
FLA2-protein complex	−34.4 ± 1.8	−14.89 ± 16.74	22.09 ± 2.31	−3.29 ± 0.08	−36.9 ± 2.58	18.8 ± 2.3	−18.1 ± 2.78
FLA3-protein complex	−35.61 ± 2.64	−2.4 ± 2.98	25.02 ± 2.53	−3.35 ± 0.07	−38 ± 2.74	21.67 ± 2.52	−16.33 ± 2.37
Native ligand-protein complex	−26.51 ± 2.89	−13.01 ± 7.52	24.09 ± 6.64	−3.5 ± 0.21	−39.52 ± 5.20	20.59 ± 6.55	−18.94 ± 3.2
Reference ligand-protein complex	-53.32 ± 2.84	-24.49 ± 10.15	43.17 ± 5.57	-5.58 ± 0.13	-77.8 ± 9.76	37.59 ± 5.52	-40.21 ± 6.13

https://doi.org/10.1371/journal.pone.0327862.t003

4. Discussion

The geometrical and thermodynamic parameters suggested that FLA1 exhibited a strong and stable binding to the envelope protein, characterized by RMSD, Rg, SASA, H-bonding, RDF, PCA, DCCM, and free energy analysis throughout the 100 ns simulation period. These findings hinted that FLA1 may effectively inhibit the function of the envelope protein. Previous studies in which compounds with comparable docking scores targeted the same active site of the protein support this work [51,60]. However, those studies lacked detailed geometrical and thermodynamic analysis.

The promising performance of FLA1 showed potential as a lead compound for developing an antiviral drug when there is an urge for novel therapeutics due to the increasing cases of viral infection yearly. However, it is significant to recognize the limitations of a computational-only approach. While the *in silico* approach provides valuable insight into molecular interactions, stability, and toxicity, which helps to identify the potential target compound, they do not account for bioavailability, metabolic stability, or off-target effects, which are crucial for real-world efficacy. Therefore, further studies are required to validate *in silico* work, including *in vitro* assays to validate antiviral activity and cytotoxicity. Later, *in vivo* studies will evaluate pharmacokinetics and therapeutic potential. These steps are essential to translate the computational promise of FLA1 into a viable antiviral agent.

5. Conclusions

This study provides valuable computational data on the prospects of flavonoids as inhibitors of the dengue virus envelope (E) protein. FLA1 was identified to possess the highest binding affinity and stability among the compounds screened, confirmed through molecular docking and molecular dynamics simulations. Key stability parameters, including RMSD, RMSF, Rg, SASA, hydrogen bond count, and RDF, indicated a stabilized ligand-protein complex. Additionally, PCA and DCCM analysis revealed significant conformational stability and dynamic correlations, respectively, that also supported the effectiveness of FLA1. Binding free energy calculations (MM/PBSA) reconfirmed its tight binding to the target protein, while ADMET profiling suggested favourable pharmacokinetic properties. These findings designate FLA1 as a promising hit compound for dengue antiviral drug development, and its therapeutic efficacy must be confirmed with additional experimentation on *in vitro* and *in vivo*.

Supporting information

S1 Fig. Ramachandran plot of DENV-2 E protein (PDB ID: 1OKE).
(TIF)

S2 Fig. Molecular structure of top 3 flavonoids, Native ligand, and Reference ligand.
(TIF)

S3 Fig. Ligand docking position in the cavity with a hydrophobic surface (a) FLA1, (b) FLA2, (c) FLA3, (d) Native ligand, and (e) Reference ligand complexes.
(TIF)

S4 Fig. PCA analysis calculation of three eigenvalues (PC1, PC2, and PC3) for the (a) FLA1, (b) FLA2, (c) FLA3, (d) Native ligand, and (e) Reference ligand complexes.
(TIF)

S5 Fig. DCCM plots for the (a) FLA1, (b) FLA2, (c) FLA3, (d) native ligand, and (e) Reference ligand complexes.
(TIF)

S6 Fig. Changes in the binding free energy of different protein adducts with (a) FLA1, (b) FLA2, (c) FLA3, (d) Native ligand, and (e) Reference ligand, red indicates the moving average.
(TIF)

S7 Fig. MM/PBSA free energy contributions of different energies to the binding energy. (a) FLA1, (b) FLA2, (c) FLA3, (d) native ligand, (e) Reference ligand, from the last 20 ns stable trajectories of the protein-ligand complexes.
(TIF)

S8 Fig. MM/PBSA free energy partial contribution of the active amino acids and ligands to the binding free energy of (a) FLA1, (b) FLA2, (c) FLA3, (d) Native ligand, and (e) Reference ligand complexes.
(TIF)

S9 Fig. MM/PBSA the free energy of (a) FLA1, (b) FLA2, (c) FLA3, (d) Native ligand, and (e) Reference ligand complexes over the last 20 ns of the stable trajectory. A heat-map showing residue-wise contributions per frame of the simulation.
(TIF)

S1 Table. Toxicity from protox-III.
(DOCX)

S2 Table. Drug-Likeness Properties of hit candidates and reference drug through the Swiss ADME Server.
(DOCX)

S3 Table. ADMET properties from ADMETlab 2.0.
(DOCX)

S4 Table. Toxicity from ADMETlab 2.0.
(DOCX)

S5 Table. Toxicity from the pkCSM server.
(DOCX)

Acknowledgments

The authors would like to acknowledge the IT Innovation Centre, Tribhuvan University, Kirtipur, Kathmandu, Nepal.

Author contributions

Conceptualization: Achyut Adhikari.

Data curation: Amar Waiba, Tika Ram Lamichhane, Madhav Prasad Ghimire.

Formal analysis: Amar Waiba, Anuraj Phunyal, Ashish Phuyal, Achyut Adhikari.

Investigation: Amar Waiba.

Methodology: Amar Waiba.

Resources: Amar Waiba.

Software: Amar Waiba.

Supervision: Achyut Adhikari.

Validation: Amar Waiba.

Visualization: Amar Waiba.

Writing – original draft: Amar Waiba, Anuraj Phunyal.

Writing – review & editing: Amar Waiba, Anuraj Phunyal, Tika Ram Lamichhane, Madhav Prasad Ghimire, Hari Nyaupane, Achyut Adhikari.

References

1. Bhatt S, Gething PW, Brady OJ, Messina JP, Farlow AW, Moyes CL, et al. The global distribution and burden of dengue. Nature. 2013;496(7446):504–7. https://doi.org/10.1038/nature12060 PMID: 23563266
2. Guzman MG, Harris E. Dengue. Lancet. 2015;385(9966):453–65. https://doi.org/10.1016/S0140-6736(14)60572-9 PMID: 25230594
3. Mohapatra RK, Bhattacharjee P, Desai DN, Kandi V, Sarangi AK, Mishra S, et al. Global health concern on the rising dengue and chikungunya cases in the American regions: countermeasures and preparedness. Health Sci Rep. 2024;7(1):e1831. https://doi.org/10.1002/hsr2.1831 PMID: 38274135
4. Hung TM, Shepard DS, Bettis AA, Nguyen HA, McBride A, Clapham HE, et al. Productivity costs from a dengue episode in Asia: a systematic literature review. BMC Infect Dis. 2020;20(1):393. https://doi.org/10.1186/s12879-020-05109-0 PMID: 32493234
5. Kalayanarooj S. Clinical manifestations and management of Dengue/DHF/DSS. Trop Med Health. 2011;39(4 Suppl):83–7. https://doi.org/10.2149/tmh.2011-S10 PMID: 22500140
6. Guzman MG, Alvarez M, Halstead SB. Secondary infection as a risk factor for dengue hemorrhagic fever/dengue shock syndrome: an historical perspective and role of antibody-dependent enhancement of infection. Arch Virol. 2013;158(7):1445–59. https://doi.org/10.1007/s00705-013-1645-3 PMID: 23471635
7. Kaptein SJ, Neyts J. Towards antiviral therapies for treating dengue virus infections. Curr Opin Pharmacol. 2016;30:1–7. https://doi.org/10.1016/j.coph.2016.06.002 PMID: 27367615
8. Low JGH, Ooi EE, Vasudevan SG. Current status of dengue therapeutics research and development. J Infect Dis. 2017;215(suppl_2):S96–102. https://doi.org/10.1093/infdis/jiw423 PMID: 28403438
9. Aguiar M, Stollenwerk N, Halstead SB. The impact of the newly licensed dengue vaccine in endemic countries. PLoS Negl Trop Dis. 2016;10(12):e0005179. https://doi.org/10.1371/journal.pntd.0005179 PMID: 28002420
10. Guy B, Barrere B, Malinowski C, Saville M, Teyssou R, Lang J. From research to phase III: preclinical, industrial and clinical development of the Sanofi Pasteur tetravalent dengue vaccine. Vaccine. 2011;29(42):7229–41. https://doi.org/10.1016/j.vaccine.2011.06.094 PMID: 21745521
11. Diaz-Quijano FA, Siqueira de Carvalho D, Raboni SM, Shimakura SE, Maron de Mello A, Vieira da Costa-Ribeiro MC, et al. Effectiveness of mass dengue vaccination with CYD-TDV (Dengvaxia®) in the state of Paraná, Brazil: integrating case-cohort and case-control designs. Lancet Reg Health Am. 2024;35:100777. https://doi.org/10.1016/j.lana.2024.100777 PMID: 38807985
12. Yu L, Nomaguchi M, Padmanabhan R, Markoff L. Specific requirements for elements of the 5' and 3' terminal regions in flavivirus RNA synthesis and viral replication. Virology. 2008;374(1):170–85. https://doi.org/10.1016/j.virol.2007.12.035 PMID: 18234265
13. Alayli F, Scholle F. Dengue virus NS1 enhances viral replication and pro-inflammatory cytokine production in human dendritic cells. Virology. 2016;496:227–36. https://doi.org/10.1016/j.virol.2016.06.008 PMID: 27348054
14. Perera R, Kuhn RJ. Structural proteomics of dengue virus. Curr Opin Microbiol. 2008;11(4):369–77. https://doi.org/10.1016/j.mib.2008.06.004 PMID: 18644250
15. Rey FA, Heinz FX, Mandl C, Kunz C, Harrison SC. The envelope glycoprotein from tick-borne encephalitis virus at 2 A resolution. Nature. 1995;375(6529):291–8. https://doi.org/10.1038/375291a0 PMID: 7753193
16. Heinz FX, Allison SL. The machinery for flavivirus fusion with host cell membranes. Curr Opin Microbiol. 2001;4(4):450–5. https://doi.org/10.1016/s1369-5274(00)00234-4 PMID: 11495810
17. Fritz R, Stiasny K, Heinz FX. Identification of specific histidines as pH sensors in flavivirus membrane fusion. J Cell Biol. 2008;183(2):353–61. https://doi.org/10.1083/jcb.200806081 PMID: 18936253
18. Kampmann T, Mueller DS, Mark AE, Young PR, Kobe B. The role of histidine residues in low-pH-mediated viral membrane fusion. Structure. 2006;14(10):1481–7. https://doi.org/10.1016/j.str.2006.07.011 PMID: 17027497
19. Bressanelli S, Stiasny K, Allison SL, Stura EA, Duquerroy S, Lescar J, et al. Structure of a flavivirus envelope glycoprotein in its low-pH-induced membrane fusion conformation. EMBO J. 2004;23(4):728–38. https://doi.org/10.1038/sj.emboj.7600064 PMID: 14963486
20. Modis Y, Ogata S, Clements D, Harrison SC. A ligand-binding pocket in the dengue virus envelope glycoprotein. Proc Natl Acad Sci U S A. 2003;100(12):6986–91. https://doi.org/10.1073/pnas.0832193100 PMID: 12759475
21. Zhang Y, Zhang W, Ogata S, Clements D, Strauss JH, Baker TS, et al. Conformational changes of the flavivirus E glycoprotein. Structure. 2004;12(9):1607–18. https://doi.org/10.1016/j.str.2004.06.019 PMID: 15341726
22. Allison SL, Schalich J, Stiasny K, Mandl CW, Kunz C, Heinz FX. Oligomeric rearrangement of tick-borne encephalitis virus envelope proteins induced by an acidic pH. J Virol. 1995;69(2):695–700. https://doi.org/10.1128/JVI.69.2.695-700.1995 PMID: 7529335
23. Modis Y, Ogata S, Clements D, Harrison SC. Structure of the dengue virus envelope protein after membrane fusion. Nature. 2004;427(6972):313–9. https://doi.org/10.1038/nature02165 PMID: 14737159
24. Badshah SL, Faisal S, Muhammad A, Poulson BG, Emwas AH, Jaremko M. Antiviral activities of flavonoids. Biomed Pharmacother. 2021;140:111596. https://doi.org/10.1016/j.biopha.2021.111596 PMID: 34126315
25. Cushnie TPT, Lamb AJ. Antimicrobial activity of flavonoids. Int J Antimicrob Agents. 2005;26(5):343–56. https://doi.org/10.1016/j.ijantimicag.2005.09.002 PMID: 16323269

26. Murota K, Terao J. Antioxidative flavonoid quercetin: implication of its intestinal absorption and metabolism. Arch Biochem Biophys. 2003;417(1):12–7. https://doi.org/10.1016/s0003-9861(03)00284-4 PMID: 12921774
27. Snijman PW, Swanevelder S, Joubert E, Green IR, Gelderblom WCA. The antimutagenic activity of the major flavonoids of rooibos (*Aspalathus linearis*): some dose-response effects on mutagen activation-flavonoid interactions. Mutat Res. 2007;631(2):111–23. https://doi.org/10.1016/j.mrgentox.2007.03.009 PMID: 17537670
28. Hemalika D, Chandrika U. Anti-dengue effects of medicinal plants: a review. Int J Herb Med. 2020;8(6):50–6. https://doi.org/10.22271/flora.2020.v8.i6a.706
29. Abd Kadir SL, Yaakob H, Mohamed Zulkifli R. Potential anti-dengue medicinal plants: a review. J Nat Med. 2013;67(4):677–89. https://doi.org/10.1007/s11418-013-0767-y PMID: 23591999
30. Tang LIC, Ling APK, Koh RY, Chye SM, Voon KGL. Screening of anti-dengue activity in methanolic extracts of medicinal plants. BMC Complement Altern Med. 2012;12:3. https://doi.org/10.1186/1472-6882-12-3 PMID: 22244370
31. Hanwell MD, Curtis DE, Lonie DC, Vandermeersch T, Zurek E, Hutchison GR. Avogadro: an advanced semantic chemical editor, visualization, and analysis platform. J Cheminform. 2012;4(1):17. https://doi.org/10.1186/1758-2946-4-17 PMID: 22889332
32. Schrödinger LLC, Warren DL. PyMOL. Version 2.4.0.
33. Morris GM, Huey R, Lindstrom W, Sanner MF, Belew RK, Goodsell DS, et al. AutoDock4 and AutoDockTools4: automated docking with selective receptor flexibility. J Comput Chem. 2009;30(16):2785–91. https://doi.org/10.1002/jcc.21256 PMID: 19399780
34. Colovos C, Yeates TO. Verification of protein structures: patterns of nonbonded atomic interactions. Protein Sci. 1993;2(9):1511–9. https://doi.org/10.1002/pro.5560020916 PMID: 8401235
35. Banerjee P, Kemmler E, Dunkel M, Preissner R. ProTox 3.0: a webserver for the prediction of toxicity of chemicals. Nucleic Acids Res. 2024;52(W1):W513–20. https://doi.org/10.1093/nar/gkae303 PMID: 38647086
36. Daina A, Michielin O, Zoete V. SwissADME: a free web tool to evaluate pharmacokinetics, drug-likeness and medicinal chemistry friendliness of small molecules. Sci Rep. 2017;7:42717. https://doi.org/10.1038/srep42717 PMID: 28256516
37. Pires DEV, Blundell TL, Ascher DB. pkCSM: predicting small-molecule pharmacokinetic and toxicity properties using graph-based signatures. J Med Chem. 2015;58(9):4066–72. https://doi.org/10.1021/acs.jmedchem.5b00104 PMID: 25860834
38. Xiong G, Wu Z, Yi J, Fu L, Yang Z, Hsieh C, et al. ADMETlab 2.0: an integrated online platform for accurate and comprehensive predictions of ADMET properties. Nucleic Acids Res. 2021;49(W1):W5–14. https://doi.org/10.1093/nar/gkab255 PMID: 33893803
39. Tian W, Chen C, Lei X, Zhao J, Liang J. CASTp 3.0: computed atlas of surface topography of proteins. Nucleic Acids Res. 2018;46(W1):W363–7. https://doi.org/10.1093/nar/gky473 PMID: 29860391
40. Trott O, Olson AJ. AutoDock Vina: improving the speed and accuracy of docking with a new scoring function, efficient optimization, and multithreading. J Comput Chem. 2010;31(2):455–61. https://doi.org/10.1002/jcc.21334 PMID: 19499576
41. Biovia DS. Discovery studio visualizer. San Diego, CA, USA: Dassault Systèmes; 2021.
42. Abraham MJ, Murtola T, Schulz R, Páll S, Smith JC, Hess B, et al. GROMACS: high performance molecular simulations through multi-level parallelism from laptops to supercomputers. SoftwareX. 2015;1–2:19–25. https://doi.org/10.1016/j.softx.2015.06.001
43. Bjelkmar P, Larsson P, Cuendet MA, Hess B, Lindahl E. Implementation of the CHARMM force field in GROMACS: analysis of protein stability effects from correction maps, virtual interaction sites, and water models. J Chem Theory Comput. 2010;6(2):459–66. https://doi.org/10.1021/ct900549r PMID: 26617301
44. Zoete V, Cuendet MA, Grosdidier A, Michielin O. SwissParam: a fast force field generation tool for small organic molecules. J Comput Chem. 2011;32(11):2359–68. https://doi.org/10.1002/jcc.21816 PMID: 21541964
45. Basconi JE, Shirts MR. Effects of temperature control algorithms on transport properties and kinetics in molecular dynamics simulations. J Chem Theory Comput. 2013;9(7):2887–99. https://doi.org/10.1021/ct400109a PMID: 26583973
46. Phunyal A, Adhikari A, Adhikari Subin J. In silico exploration of potent flavonoids for dengue therapeutics. PLoS One. 2024;19(12):e0301747. https://doi.org/10.1371/journal.pone.0301747 PMID: 39666626
47. Gyawali K, Maharjan R, Acharya A, Khanal M, Ghimire MP, Lamichhane TR. Identification of catechin as main protease inhibitor of SARS-CoV-2 Omicron variant using molecular docking, molecular dynamics, PCA, DCCM, MM/GBSA and ADMET profiling. Nat Prod Res. 0(0):1–8. https://doi.org/10.1080/14786419.2024.2421907 pmid:39487761.
48. Ramírez D, Caballero J. Is it reliable to take the molecular docking top scoring position as the best solution without considering available structural data?. Molecules. 2018;23(5):1038. https://doi.org/10.3390/molecules23051038 PMID: 29710787
49. Rayamajhi A, Karki D, Phunyal A, Sapkota A, Adhikari B, Adhikari A. Phytochemical profiling from Dioscorea bulbifera L. bulbils using LC-MS, proximate analysis and antidiabetic activity: in vitro and in silico approaches. Int J Food Prop. 2024;27(1):1396–414. https://doi.org/10.1080/10942912.2024.2410469
50. Hanson G, Adams J, Kepgang DIB, Zondagh LS, Tem Bueh L, Asante A, et al. Machine learning and molecular docking prediction of potential inhibitors against dengue virus. Front Chem. 2024;12:1510029. https://doi.org/10.3389/fchem.2024.1510029 PMID: 39776767
51. Naresh P, Selvaraj A, Shyam Sundar P, Murugesan S, Sathianarayanan S, Namboori P K K, et al. Targeting a conserved pocket (n-octyl-β-D-glucoside) on the dengue virus envelope protein by small bioactive molecule inhibitors. J Biomol Struct Dyn. 2022;40(11):4866–78. https://doi.org/10.1080/07391102.2020.1862707 PMID: 33345726

52. Martínez L. Automatic identification of mobile and rigid substructures in molecular dynamics simulations and fractional structural fluctuation analysis. PLoS One. 2015;10(3):e0119264. https://doi.org/10.1371/journal.pone.0119264 PMID: 25816325

53. Durham E, Dorr B, Woetzel N, Staritzbichler R, Meiler J. Solvent accessible surface area approximations for rapid and accurate protein structure prediction. J Mol Model. 2009;15(9):1093–108. https://doi.org/10.1007/s00894-009-0454-9 PMID: 19234730

54. Zhang D, Lazim R. Application of conventional molecular dynamics simulation in evaluating the stability of apomyoglobin in urea solution. Sci Rep. 2017;7:44651. https://doi.org/10.1038/srep44651 PMID: 28300210

55. Chikalov I, Yao P, Moshkov M, Latombe J-C. Learning probabilistic models of hydrogen bond stability from molecular dynamics simulation trajectories. BMC Bioinformatics. 2011;12 Suppl 1(Suppl 1):S34. https://doi.org/10.1186/1471-2105-12-S1-S34 PMID: 21342565

56. Levine BG, Stone JE, Kohlmeyer A. Fast analysis of molecular dynamics trajectories with graphics processing units-radial distribution function histogramming. J Comput Phys. 2011;230(9):3556–69. https://doi.org/10.1016/j.jcp.2011.01.048 PMID: 21547007

57. Lamichhane TR, Ghimire MP. Evaluation of SARS-CoV-2 main protease and inhibitor interactions using dihedral angle distributions and radial distribution function. Heliyon. 2021;7(10):e08220. https://doi.org/10.1016/j.heliyon.2021.e08220 PMID: 34693066

58. Maharjan R, Gyawali K, Acharya A, Khanal M, Ghimire MP, Lamichhane TR. Artemisinin derivatives as potential drug candidates against Mycobacterium tuberculosis : insights from molecular docking, MD simulations, PCA, MM/GBSA and ADMET analysis. Mol Simul. 2024;50(11):717–28. https://doi.org/10.1080/08927022.2024.2346525

59. Karki D, Phunyal A, Lamichhane TR, Rayamajhi A, Sapkota A, Nyaupane H, et al. Chemical profiling, in-vitro and in silico α -glucosidase inhibition, antioxidant and antibacterial activities of Hypotrachyna cirrhata (Fr.) Hale ex Sipman. All Life. 2024;17(1). https://doi.org/10.1080/26895293.2024.2424894

60. Tambunan USF, Alkaff AH. Identification of natural products as an inhibitor of β-OG pocket binder of dengue virus envelope protein using fragment-based drug design and molecular docking approach. AIP Conf Proc. 2018;2023(1): 020059. https://doi.org/10.1063/1.5064056